On lattice dynamics, stability and acidity of zeolites

ON LATTICE DYNAMICS, STABILITY AND ACIDITY OF ZEOLITES

R.A. van Santen°+, B.W.H. van Beest+, A.J.M. de Man°

° Eindhoven University of Technology
Eindhoven
The Netherlands
+ Koninklijke/Shell Laboratory
Amsterdam
The Netherlands

INTRODUCTION

Theoretical approaches to chemical bonding and the stability of zeolites can be distinguished in quantum mechanical methods based on electronic structure calculations[1,2] and methods that start with known potentials[3].

Because of the large elementary unit cell of zeolite structures no quantum chemical calculations are available for zeolites, but a full quantum mechanical ab-initio calculation for quartz is available[4]. Otherwise the quantum mechanical approach limits itself to the study of silicate rings or clusters[1]. Quantum chemical ab-initio or semi-empirical techniques have been applied to study the relative stability of such clusters[1] as well as the acidity of protons as a function of composition[5].

In solid state chemistry extensive use is made of infinite lattice techniques, based on electrostatic potentials, modified by empirical short range potentials[3c]. The minimum lattice energy and corresponding lattice configuration are determined by relaxing the structure. Pure valence force field calculations[6] have been applied too and a combination of valence force fields and electrostatic forces has recently been used to simulate an isolated sodalite cage[7].

The empirical potentials used in infinite lattice techniques have usually been determined by fitting them such that computed structure and elasticity constants reproduce experimental values optimally. For chemical purposes potentials are required that give correct potential energy surfaces. Infrared and Raman spectra provide sensitive probes for the potentials used by comparison of computed and measured spectra.

Here we will present such an analysis for the results of infinite lattice calculations based on empirical potentials, derived for α-quartz using rigid ion as well as shell model calculations. Structures considered will be limited to zeolitic polymorphs of silica, containing only silicon and oxygen atoms. From the difference in average energy of the longitudinal and transverse optical frequencies a deduction can be made of the effective charges on the atoms forming a zeolite. However, experimental data on this difference are only available for quartz. From this the effective electrostatic field in

Guidelines for Mastering the Properties of Molecular Sieves
Edited by D. Barthomeuf *et al.*
Plenum Press, New York, 1990

the micropores of the zeolite can be estimated. The results appear to agree rather well with those based on quantum mechanical estimates[5].

We will conclude the paper with a short discussion of the impact of our results on ideas concerning the factors that determine the acidity of zeolites.

THE VIBRATIONAL DENSITY OF STATES (VDOS)

Notwithstanding the large number of SiO_2 tetrahedral units per elementary unit cell in zeolite structures, a useful approach to the basic understanding of the mode distribution can be derived from a model based on the Bethe lattice approximation. In its most simple version only a system with one SiO_2 tetrahedron per unit cell is considered. Extension to the prescribed number of SiO_2 tetrahedra per unit cell for a particular zeolite structure in combination with a factor group analysis enables a prediction of the frequency distribution of vibrational stretching modes. This has been discussed elsewhere[8]. Here we will summarize the results of the Bethe lattice considerations and use the result to analyse computed spectra from rigid ion and shell model calculations on α-quartz, silica-sodalite and silica-faujasite[3s].

The VDOS is best understood realising that the coupling of the individual SiO_2 tetrahedral modes depends on the Si-O-Si-angle ϕ. If this angle is 90° and the Si-O-Si threebody potential is ignored, the modes of the tetrahedra will not couple. Coupling is maximum at ϕ=180°. For quartz the average angle ϕ is 144°, so coupling of the modes will be significant.

Quantum mechanical[1a,1b,1p] as well as spectroscopic studies indicate that the frequency of the Si-O-Si bending modes is two orders of magnitude less than that of Si-O stretch modes. For this reason in the Bethe lattice calculations to be discussed the Si-O-Si threebody potential is ignored. The situation is different for the O-Si-O bending modes. This bending mode frequency is of the order of 300 cm^{-1}. The tetrahedral coordination of oxygen atoms around silicon requires the O-Si-O threebody to be rather stiff. In the Bethe lattice calculations to be discussed it is assumed that

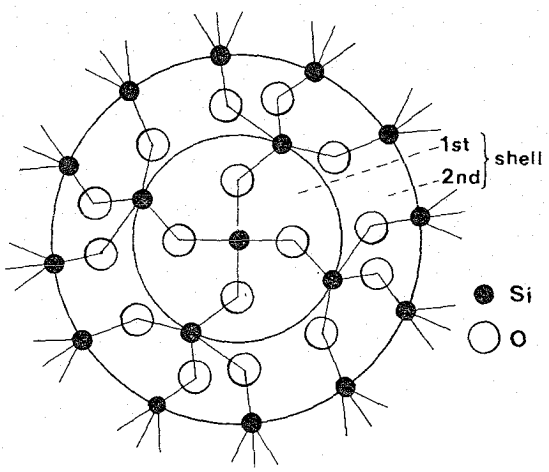

Figure 1. The Bethe lattice of Si-O-Si oscillators.

the O-Si-O angle is rigid. A discussion of the calculational details is given in ref. (8). Here we will give an outline of the results.

In the Bethe lattice method the fundamental bonding unit is the Si-O-Si bond. Figure 1 illustrates the Bethe lattice approximation, figures 2 and 3 the resulting VDOS's. Symmetric and asymmetric Si-O-Si stretching modes are formed with frequency differences depending on the Si-O-Si angle. The average frequency depends on the Si-O stretch frequency in the uncoupled system. The symmetric and asymmetric Si-O-Si modes mix according to tetrahedral symmetry because they are coupled by

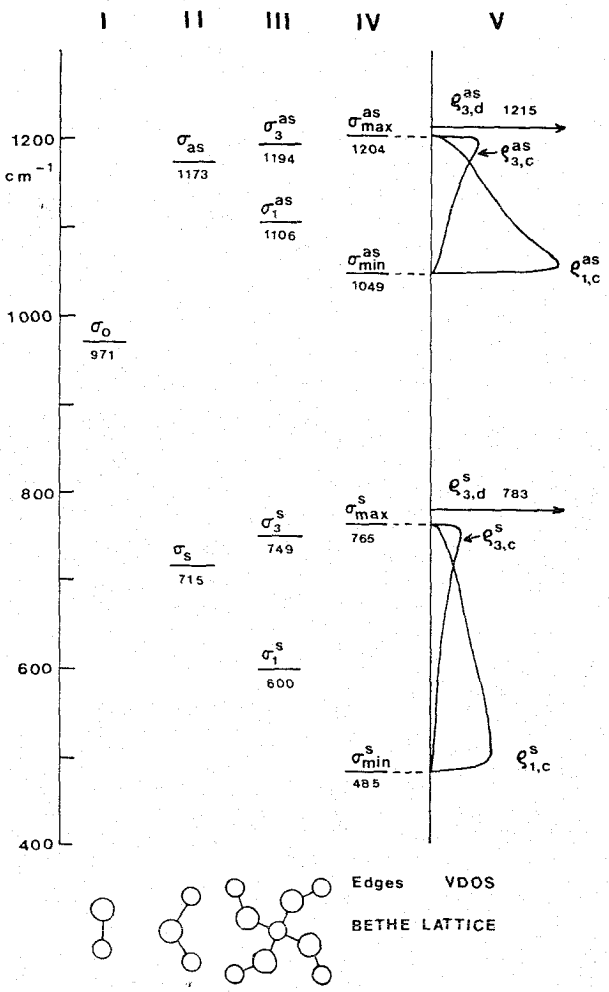

Figure 2. The VDOS of stretching modes for a Si-O-Si angle ϕ of 149°.
Column I: Wave number σ_0 of the uncoupled Si-O oscillator.
Column II: Wave numbers σ_{as} and σ_s of the "free" Si-O-Si oscillator.
Column III: Wave numbers of four tetrahedrally arranged Si-O-Si oscillators.
Column IV: VDOS of the Bethe lattice of Si-O-Si oscillators.

the same silicon atom. Because of the large energy difference between the symmetric and asymmetric Si-O-Si modes and the small coupling of the modes, due to the closeness of the O-Si-O angle to 90°, the symmetric and asymmetric Si-O-Si stretching modes can be considered to remain independent from each other in the tetrahedral coordination around the silicon atom. Eight modes are found, split according to T_d symmetry (figs. 2 and 3).

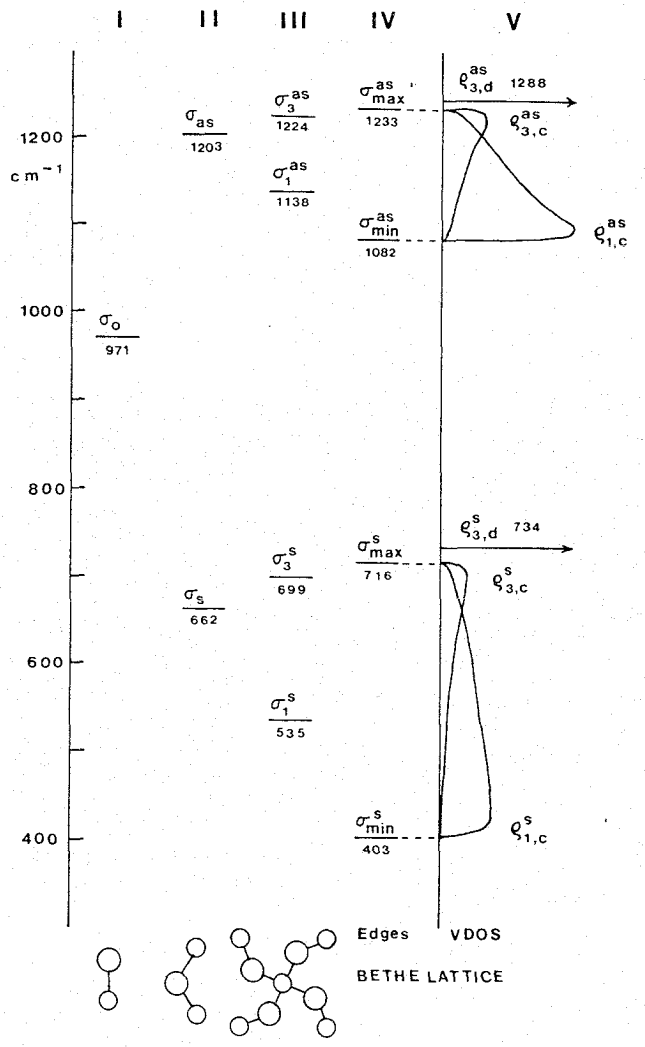

Figure 3. The VDOS of stretching modes for a Si-O-Si angle ϕ of 180°.
Column I: Wave number σ_0 of the uncoupled Si-O oscillator.
Column II: Wave numbers σ_{as} and σ_s of the "free" Si-O-Si oscillator.
Column III: Wave numbers of four tetrahedrally arranged Si-O-Si oscillators.
Column IV: VDOS of the Bethe lattice of Si-O-Si oscillators.

To form the Bethe lattice the Si-O-Si modes have to be connected to the other modes *via* silicon atoms in a second shell. This is continued *ad infinitum* with the essential approximation that no cross connections are made between the Si-O-Si modes. So ring formation between the tetrahedra is ignored. This seems a rather unphysical approximation. However it can be shown[9,10] that one can systematically improve on it to incorporate structural details. In the absence of cross connections and maintaining the approximation that the asymmetric and symmetric Si-O-Si modes remain uncoupled, the resulting set of dynamic equations can be analytically solved, with the resulting VDOS given in figures 2d and 3d. One finds that the four Si-O stretching vibrations of the isolated SiO_4 tetrahedron transform into two localized and two delocalized stretching vibrations. One set of localized and delocalized modes can be considered to originate from the antisymmetric Si-O-Si stretching vibrations located between 900 and 1200 cm^{-1}. The other set of localized and delocalized modes can be considered to be derived from the symmetric Si-O-Si stretching vibrations and is found between 450 and 850 cm^{-1}. In the case a structure contains n SiO_2 tetrahedral units per elementary unit cell $2n$ localized and $2n$ delocalized modes are found. The number of optically active modes is found by an adapted factor group analysis method[8,3g].

We will now analyse experimental and computed spectra on the basis of Bethe lattice model results. Figures 4 and 5 show a comparison of experimental and computed infrared spectra for α-quartz. Details of the computations are given in ref. (3g). In figure 4 results of rigid ion calculations are compared, in figure 5 results of shell model calculations.

Clearly computed and experimental spectra do not agree very well if results of the rigid ion calculations are compared. Especially the appearance of intensity in the

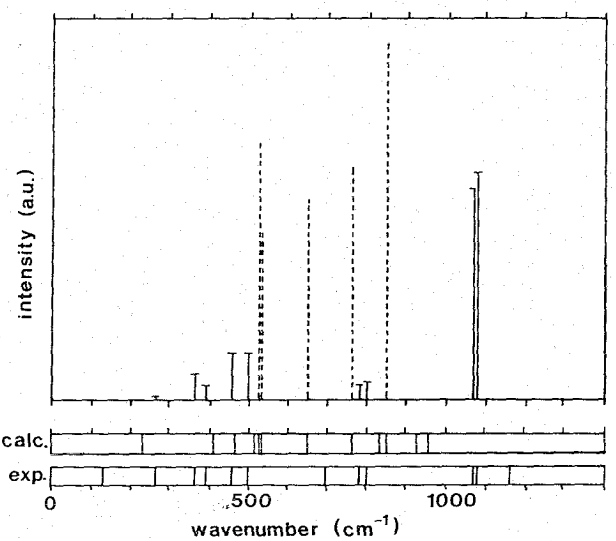

Figure 4. Infrared spectra of α-quartz. Solid lines: experimental[11] frequencies; Broken lines: calculated according to the rigid ion model.

"quartz frequency gap" between 500 and 700 cm^{-1} is of concern.

The shell model calculations (fig. 5) reproduce an intensity free "quartz frequency gap". Also the grouping of computed and measured bands corresponds rather well. Agreement of modes below 500 cm^{-1}, the vibrations derived from the O-Si-O bending modes, is satisfactory. The average position of the calculated stretching modes above 800 cm^{-1} appears to be too low. Also the difference in energy of the two high frequency stretching modes (~900 cm^{-1}) and the low frequency stretching modes (~800 cm^{-1}) is much smaller than the experimental value. The corresponding experimental high frequency stretching modes are at approximately 1080 cm^{-1} whereas the experimental low frequency stretching modes are found at approximately 800 cm^{-1}. The high frequency modes correspond to the asymmetrically coupled Si-O stretching modes. The low frequency modes correspond to the symmetrically coupled Si-O stretching modes. The difference as well as the average value of these modes depends on the value of the Si-O stretch frequency. One concludes that bending and stretch frequencies computed according to the shell model are in much better agreement with experiment than those derived from the rigid ion calculations. However, the Si-O stretch mode frequency computed according to the shell model is still too small.

In figures 6 and 7 a comparison between computed shell model and experimental lattice infrared spectra is given for silica-sodalite and silica-faujasite. The discrepancies between experimental and computed data are similar for α-quartz and again agreement is rather good in the bending frequency region.

In the next section a detailed analysis of the reasons for the differences in results of rigid ion and shell model calculations is given. Also of interest for this discussion is a comparison of computed differences in frequency of longitudinal (LO) optical and transversal optical (TO) modes. For α-quartz such a comparison is shown in fig. 8. One observes a much larger difference in frequencies of corresponding LO and TO

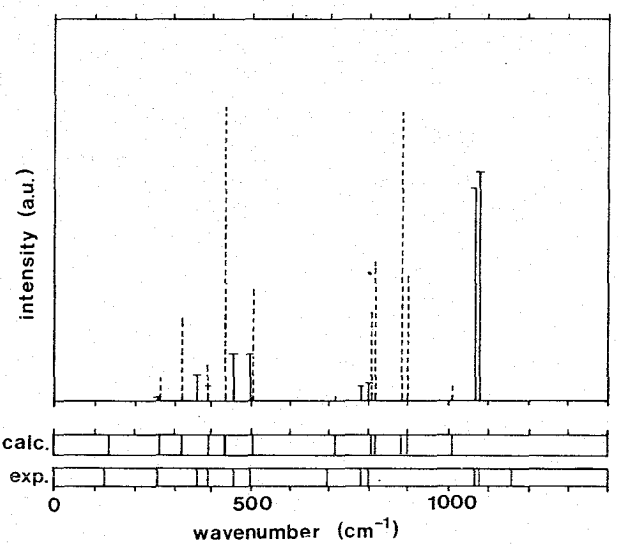

Figure 5. Infrared spectra of α-quartz. Solid lines: experimental[11] frequencies; Broken lines: calculated according to the shell model.

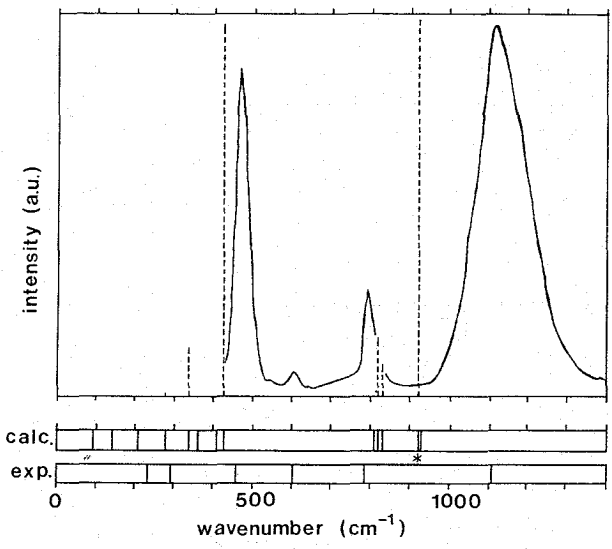

Figure 6. Infrared spectra of sodalite (spacegroup $P\bar{4}3n$ or T_d^4).
Solid lines: experimental frequencies;
Broken lines: calculated according to the shell model.

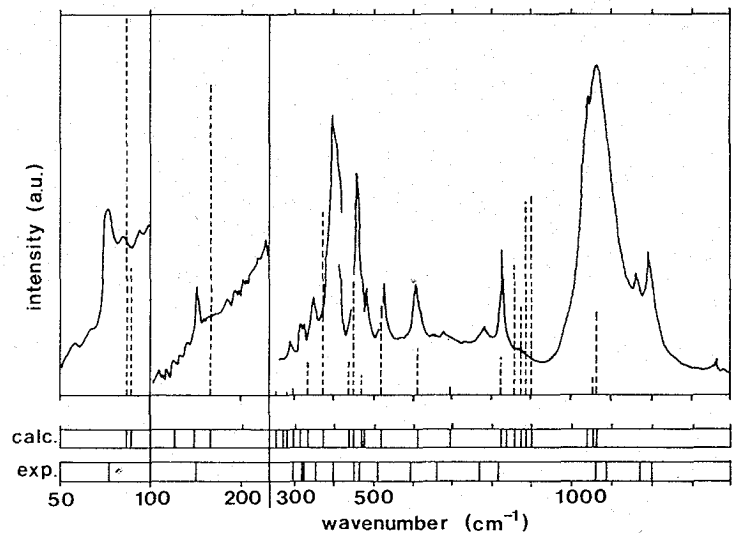

Figure 7. Infrared spectra of faujasite (spacegroup Fd3m or O_h^7).
Solid lines: experimental frequencies;
Broken lines: calculated according to the shell model.

modes for the rigid ion and shell model calculations than seen in the experiment. The largest differences are found in the stretching frequency regime.

RIGID ION versus SHELL MODEL CALCULATIONS

For a detailed derivation of the equations of motion to be used in the rigid ion and the shell model, we refer to the excellent monograph of P. Brüesch[12]. An extensive treatment can be found in the book of Maraduddin *e.a.*[13]. Here we will summarize some essential results and use them to interprete the difference between rigid ion and shell model results. This will be used to indicate how further improvements

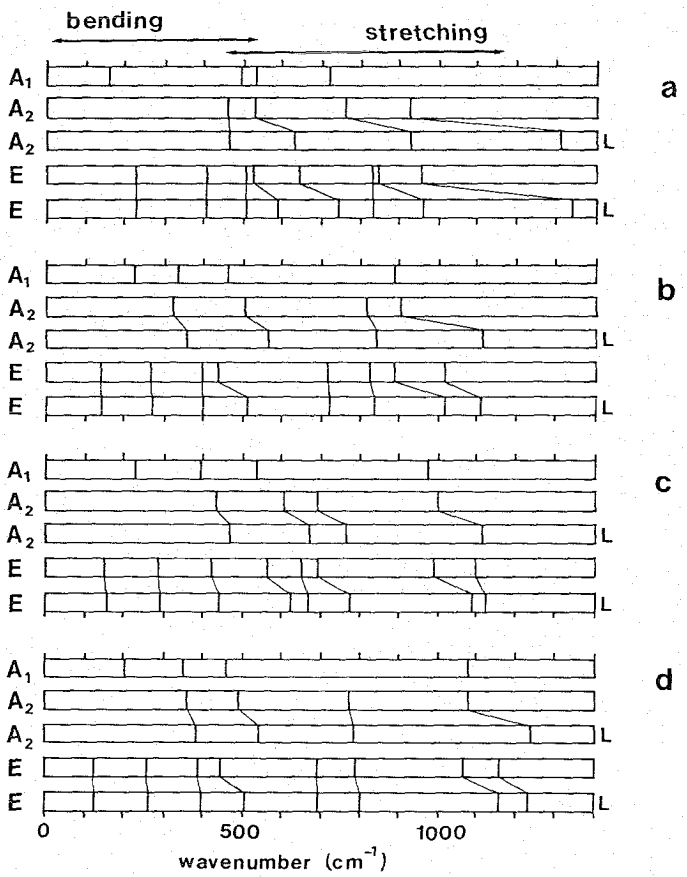

Figure 8. TO-LO splitting of α-quartz.
a: Calculated according to the rigid ion model;
b: Calculated according to the shell ion model;
c: Calculated according to the potential derived[15] from ab-initio calculations of Tsuneyuki[14];
d: Experimental values, as collected by Striefler and Barsch[16];

can be made. In the rigid ion as well as the shell model calculations used here, full formal charges on the cations are used to derive the electrostatic potential. In the rigid ion method to the Coulomb potential a Born repulsion and a van der Waals attraction term is added. The parameters used are given in ref. (3e), and were found by optimisation studies of calculated lattice constants and elastic constants for computed minimum energy structures and corresponding experimental values of α-quartz. The vibrational modes were calculated within the harmonic approximation.

It is useful to quote[12] the resulting rigid ion equations of motion for a diatomic cubic alkali-halide crystal having only a Coulomb- and a nearest neighbour short range interaction.

One finds (for a zero wavevector $\vec{k}$):

$$\mu\ddot{\mathrm{w}}_{\mathrm{LO}} + S\mathrm{w}_{\mathrm{LO}} = Ze\beta_{\mathrm{LO}}P = -\frac{8\pi}{3}\frac{Z^2e^2}{v_a}\mathrm{w}_{\mathrm{LO}} \tag{1a}$$

$$\mu\ddot{\mathrm{w}}_{\mathrm{TO}} + S\mathrm{w}_{\mathrm{TO}} = Ze\beta_{\mathrm{TO}}P = \frac{4\pi}{3}\frac{Z^2e^2}{v_a}\mathrm{w}_{\mathrm{TO}} \tag{1b}$$

where w is the relative displacement of the two ions, μ the reduced mass, S the force constant derived from the short range potential, Z the charge of the cations, P the polarization and v_a is the volume per oscillator.
β and P are given by:

$$\beta_{\mathrm{LO}} = -\frac{8\pi}{3} \tag{2a}$$

$$\beta_{\mathrm{TO}} = \frac{4\pi}{3} \tag{2b}$$

and:

$$P = \frac{Ze\mathrm{w}}{v_a} \tag{3}$$

The expressions for the LO and TO frequencies ω are:

$$\mu\omega_{\mathrm{LO}}^2 = S + \frac{8\pi Z^2e^2}{3v_a} \tag{4a}$$

$$\mu\omega_{\mathrm{TO}}^2 = S - \frac{4\pi Z^2e^2}{3v_a} \tag{4b}$$

According to the rigid ion method, the difference between longitudinal and transversal optical frequencies relates directly to the charge of the ions.

The corresponding expressions according to the shell model are:

$$\mu\omega_{\mathrm{LO}}^2 = S' + \frac{8\pi(Z'_{\mathrm{eff}})^2e^2}{3v_a\epsilon(\infty)} \tag{5a}$$

$$\mu\omega_{\mathrm{TO}}^2 = S' - \frac{4\pi(Z'_{\mathrm{eff}})^2e^2}{3v_a\epsilon(\infty)} \tag{5b}$$

Two new constants are introduced: the effective charge Z'_{eff} and the dielectric constant for infinite frequency $\epsilon(\infty)$ (see Appendix for a derivation).

The equations of motion become :

$$\mu\ddot{w}_{LO} + S' w_{LO} = Z'_{eff} E_{LO} = \frac{8\pi}{3} \frac{(Z'_{eff})^2 e^2}{\epsilon(\infty) v_a} \tag{6a}$$

$$\mu\ddot{w}_{TO} + S' w_{TO} = Z'_{eff} E_{TO} = -\frac{4\pi}{3} \frac{(Z'_{eff})^2 e^2}{\epsilon(\infty) v_a} \tag{6b}$$

and

$$E_{LO} = \beta_{LO} P_{LO} = -\frac{4\pi}{3} \frac{(Z'_{eff})^2 e^2}{\epsilon(\infty) v_a} w_{LO} \tag{7a}$$

$$E_{TO} = \beta_{TO} P_{TO} = \frac{8\pi}{3} \frac{(Z'_{eff})^2 e^2}{\epsilon(\infty) v_a} w_{TO} \tag{7b}$$

According to the shell model the expression for the dielectric constant becomes:

$$\epsilon(\omega) = \epsilon(\infty) + \frac{4\pi (Z'_{eff})^2 e^2}{\mu v_a (\omega_{TO}^2 - \omega^2)} \tag{8}$$

$\epsilon(\infty)$ follows from the Clausius-Mosotti relation:

$$\frac{\epsilon(\infty) - 1}{\epsilon(\infty) + 2} = \frac{4\pi \alpha^*_{eff}}{3 v_a} \tag{9}$$

α^*_{eff} being the effective polarizability per cation-anion pair.
Since

$$\omega_{LO}^2 - \omega_{TO}^2 = \frac{4\pi (Z'_{eff})^2}{\mu v_a \epsilon(\infty)} = \omega^2_{plasmon} \tag{10}$$

and $\epsilon(\infty)$ follows from the calculations, Z'_{eff} can be derived. In table 1 $\omega_{plasmon}$, Z'_{eff} and $\epsilon(\infty)$ are listed as computed and used for α-quartz, silica-sodalite and silica-faujasite.

As outlined in the appendix the value of Z'_{eff} results from a comparison of rigid ion and shell model calculations. The main difference between the shell model approximation and the rigid ion model is the introduction of an effective polarizability (eq. 9) in the shell model. Since in the rigid ion model $\epsilon(\infty) = 1$, the electrostatic interactions decrease in the shell model because of the larger dielectric constant. The electrostatic interaction is also reduced in the shell model by the lower value of Z'_{eff}. In the shell model polarization is included by coupling the negatively charged electron clouds by force constants k with the positively charged cores. The electron clouds of different ions are coupled with force constants f.
Z'_{eff} relates to the rigid ion charges by:

$$Z'_{eff} = \frac{\epsilon(\infty) + 2}{3} \left(Z_{core} + \frac{Z_{electrons} \frac{k}{f}}{1 + \frac{k}{f}} \right) = \frac{\epsilon(\infty) + 2}{3} Z^* \tag{11}$$

Since in the rigid ion model $\epsilon(\infty) = 1$ and $k = \infty$, Z'_{eff} reduces to $Z_{core} + Z_{electrons}$. Clearly in the shell model Z'_{eff} is significantly reduced. Table 1 shows this reduction of Z'_{eff}.

The improvements of the shell model calculations compared to the rigid ion calculations derive from the significant reduction of the Coulomb term. As a result

Table 1. Calculation of Z'_{eff}/Z.

Species	Shell model			Rigid ion model			Z'_{eff}/Z
	v_a	$\epsilon(\infty)$	ω_{plasmon}	v_a	$\epsilon(\infty)$	ω_{plasmon}	
	Å^3		cm^{-1}	Å^3		cm^{-1}	
α-quartz*	36.107	2.1163	366.80	42.367	1.0000†	557.80	0.8831
α-quartz°	36.107	2.1397	254.24	42.367	1.0000†	394.43	0.8704
Sodalite	56.168	1.6992	166.73	59.110	1.0000†	248.50	0.8525
Faujasite	74.066	1.5030	107.53	62.51	1.0000†	149.98	0.8384
α-quartz$^{\ddagger *}$	40.35	1.0000†	342.94				
α-quartz$^{\ddagger \circ}$	40.35	1.0000†	242.49				
α-quartz$^{\times *}$	37.66	2.383	139.57				
α-quartz$^{\times \circ}$	37.66	2.356	98.55				

† : In the rigid ion model the high frequency dielectric constants are exactly one.
* : The zz-component of the dielectric tensor and the shift of the A_2 modes are taken;
$^\circ$: The xx-component of the dielectric tensor and the splitting of the E modes are taken.
‡ : Calculated[15] with the potential of ref. 14.
$^\times$: Experimental[46] value.
The calculations are made with a length of the wavevectors $\vec{k}$ of about 0.001 reciprocal lattice units.

the potential fitting procedure becomes much more sensitive to a proper choice of S, with the improved spectral predictions as a result.

It is interesting that the form of the equations of motion to solve according to the rigid ion or shell model is very similar. The shell model provides an equation of motion if the values of Z'_{eff} and $\epsilon(\infty)$ are known. Comparison of Z'_{eff} used in the calculations and that derived from the values found in quantum mechanical calculations (see table 1 and figure 11a), show considerable discrepancies. Interestingly however the shell model effective charges have significantly decreased compared to the full formal charges. The effective charge decreases with decreasing density. This is expected on the basis of the lower Madelung potentials.

The infrared spectra of α-quartz computed according to the rigid ion model with an effective charge Z'_{eff} and force constants derived from an ab-initio calculation on a $SiO_4H_4^+$ cluster[14] gives improved results[15] compared to the rigid ion model calculations based on empirical potentials (see fig. 9). Comparing experimental and computed plasmon frequencies shows rather good agreement if the computed values are divided by $\epsilon(\infty)$.

The small experimental values for the plasmon frequencies of α-quartz[16] (see table 1) indicate that chemical bonding in the silica polymorphs is dominated by the short range interactions. One can estimate the ratio of the Coulomb force constant and short range (two-body) force constant from the average energy of the longitudinal and transverse optical frequencies. For α-quartz this ratio is about 0.008. Indeed the calculated shell model lattice energies for α-quartz, silica-sodalite and silica-faujasite indicate a maximum difference in lattice energy of ~20 kJ/mol SiO_2 (table 2). In view

Table 2. Contributions to lattice energy (kJ/mol SiO_2).

Species	Model	Coulomb	Two-body	Three body	Total
α-quartz	ref. 14†	-5419.6	5419.56	0.0†	-5183.6
	Rigid ion	-15412.8	3447.0	9.8	-11956.1
	Shell	-15298.7	2998.2	116.8	-12417.3
	(diff.)	-114.1	448.8	-107.0	461.2
Faujasite	Rigid ion	-15310.9	3402.6	3.4	-11911.7
	Shell	-15235.6	3020.1	204.0	-12397.5
	(diff.)	-102.3	382.5	-200.6	485.5

(diff.): Difference between Rigid ion and Shell model.
†: The potential of Tsuneyuki does not contain a threebody term and uses partial charges (0.6 times the formal charge).

of the much smaller differences in energy found for optimized silicon hydroxide ring systems[1b] in ab-initio calculations, the differences in lattice energy of silica zeolites mainly derive from electrostatic interactions. This is confirmed by analysis of the differences in energy using rigid ion and shell model calculations.

In a recent paper Johnson *e.a.*[17] and Patarin *e.a.*[18], comparing the experimental heats of formation of silicalite and α-quartz, find a difference of only 6 kJ/mol SiO_2. This is in agreement with the theoretical results.

In the last section implications of our finding that the long range electrostatic field has only a very small contribution to binding in silica-zeolites to the understanding of acidity will be discussed.

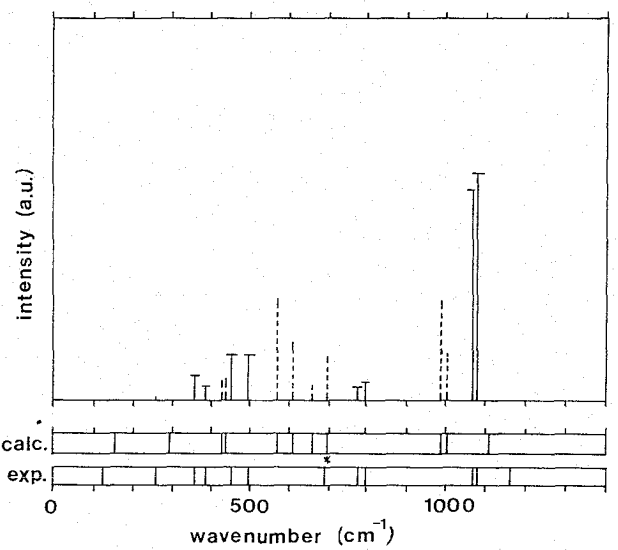

Figure 9. Infrared spectra of α-quartz. Solid lines: experimental[11] frequencies; Broken lines: calculated according to the potential derived[15] from ab-initio calculations of Tsuneyuki[14];

IMPLICATIONS FOR ACIDITY THEORY

The disagreement between the effective charges found on the basis of empirical shell model calculations and those based on potentials derived from ab-initio calculations indicates the need to use quantum chemical calculations to get reliable electrostatic field estimates.

An interesting approach along these lines is due to Goursot *e.a.*[5]. Using ab-initio quantum chemical cluster calculations they arrive at typical values of electrostatic stabilization of a proton next to an Al^{3+} containing tetrahedron of the order of 250 kcal/gat H^+.

In order to compute hydrogen bond forming properly, care has to be taken that local electric gradients are accurately computed. In addition the covalent nature of the O-H bond has to be accounted for. In order to do so for zeolites rather large clusters or embedding methods may have to be used.

To an analysis of acidity a breakdown of overall protonation into the following imaginary steps is helpful (see also ref. (2b)):

BH		$\longrightarrow$	B + H	I
B + H		$\longrightarrow$	B^- + H^+	II
H^+ + A		$\longrightarrow$	$[HA]^+$	III
B^- + H^+A		$\longrightarrow$	$B^- \cdots [HA]^+$	IV
BH + A		$\longrightarrow$	$B^- \cdots [HA]^+$	

Step I is covalent dissociation, step II is ionization, step III protonation and step IV stabilization of the protonated complex. Step II, ionization, depends strongly on the difference in electrostatic potential of an electron on the proton position, compared to an electron on the oxygen in the zeolite lattice. So for protonation, in this step not only the proton potential, but also stabilization of the negative charge on the zeolite lattice is important. The difference in potential relates to the Madelung potential of the B^-H^+ pair. Earlier we estimated differences in acidity of protons in mordenite and montmorillonite on the basis of differences in Madelung potential[19]. Of course differences in the electrostatic field the $[HA]^+$ complex experiences are of importance, but also proper calculation of the Born repulsion energy[20] of the $B^- \cdots [HA]^+$ complex. That stabilization of the protonated complex by the negatively charged zeolite wall is important, has been proposed by Kazansky[1f,2d]. Stabilization of the protonated complex by the negatively charged zeolite wall replaces hydratation of the generated ions that will occur in water.

In order to discuss the importance of electrostatic effects it is useful to consider the effect of cluster choice and zeolite lattice composition on the ionization step. Then we are interested in the difference in potential energy of an electron on the proton position and the oxygen atom.

Whereas electrostatic interactions are long range, it appears that changes in Madelung potential by the generation of surfaces[21] or vacancies[3c] remain limited to finite disturbances. Changes in electrostatic potential disappear in the third or fourth coordination shell with respect to the disturbance. Evjen[22] demonstrated that reasonable estimates of the Madelung potential can be made by choosing the charges on the neighbouring atoms such, that the total clusters remain neutral. We have shown[21] that differences in Lewis acidity of TiO_2 surfaces can be understood in a purely electrostatic model from the differences in local environment of the oxygen

atoms coordinated to the Ti ions reacting with the base. Also Madelung calculations of the lattice energy of the zeolite lattices with varying cation content indicated the dominance of short range effects[3a]. Only when cations enclosed in the zeolite channel directly contact each other large repulsive effects are observed.

Semi-empirical calculations demonstrated[23] that the effect of aluminum concentration on acidity is dominated by the number of aluminum tetrahedra neighbouring the $[_{Si-\overset{H}{O}-Al}]$ unit. The larger the number of aluminum tetrahedra next to the silicon tetrahedron, the lower the acidity. This was rationalized on basis of step II. The negative charge of the Si-O-Al bridging oxygen atom is better accomodated if its local environment becomes electron deficient. Substitution of Si^{4+} lattice ions by Al^{3+} cations has demonstrated more highly charged oxygen atoms next to neighbour tetrahedron Si ions. As a result the charge of Si decreases and it is more difficult to accomodate the negative lattice charge left upon protonation.

This is illustrated in figure 10.

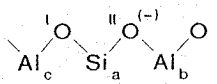

Figure 10: Oxygen sites in a alumino-silicate.

With an aluminum ion in position c, instead of a Si ion, the negative charge on the oxygen ion in position II will become larger. As a result the positive charge on the Si atom in position a will become reduced. The increased negative charge in position II and the decreased positive charge on position a will destabilize the negative charge on position I. This reduces the stability of B^- in step II. This will unfavourably affect acidity. Mortier *e.a.*[2i] have also emphasized the importance of the negative charges on the zeolite lattice oxygens.

We will analyse this using the results of fully angle and distance optimized STO-3G ab-initio calculations on three tetrahedra containing silica and alumino-silicate rings.

In figures 11 and 12 the charge distributions and equilibrium configurations are shown in the absence and presence of aluminum and compensating ions for the three-tetrahedron ring systems. The tetrahedra are connected with bridging oxygen atoms and are closed by two OH-groups. For details of the computations we refer to refs. 24 and 1b.

Relevant to theoretical computations are not only the different charges of the bridging oxygen atoms and the increase in charge with a neighbouring aluminum atom (compare *e.g.* fig. 11a, b), but also the very different charges of oxygen atoms in the hydroxyl groups. The electrostatic potential in the proton position as well as oxygen atom to which it is attached will significantly depend on the charges of the hydroxyl groups.

The OH terminated cluster has Si and Al charges nearly twice that of the hydrogen terminated clusters. The large charge differences computed for oxygen-hydroxyl charges and bridging oxygen atoms raise the question whether part of the embedding approaches using effective Madelung fields[2c,j,k] to enhance acidity, partiallly compen-

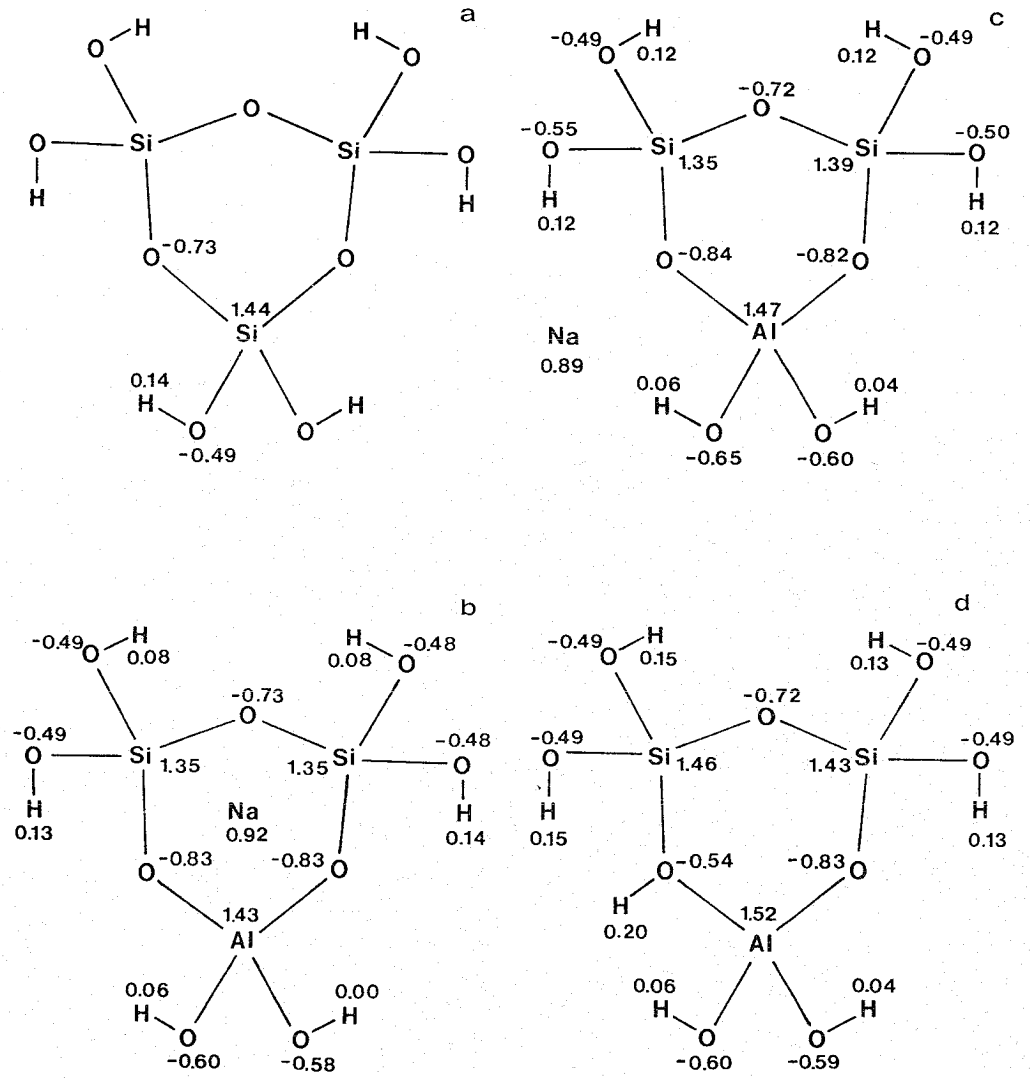

Figure 11. Charge distributions (schematic structure).
a: Aluminumfree ringsystem: $Si_3O_3(OH)_6$.
b: Na-aluminosilicate ring. Na^+ symmetrically coordinated:
$AlSi_2O_3(OH)_6^- + Na^+$.
c: Na-aluminosilicate ring. Na^+ asymmetrically coordinated:
$AlSi_2O_3(OH)_6^- + Na^+$.
d: The protonated aluminosilicate ring:
$AlSi_2O_3(OH)_6^- + H^+$.

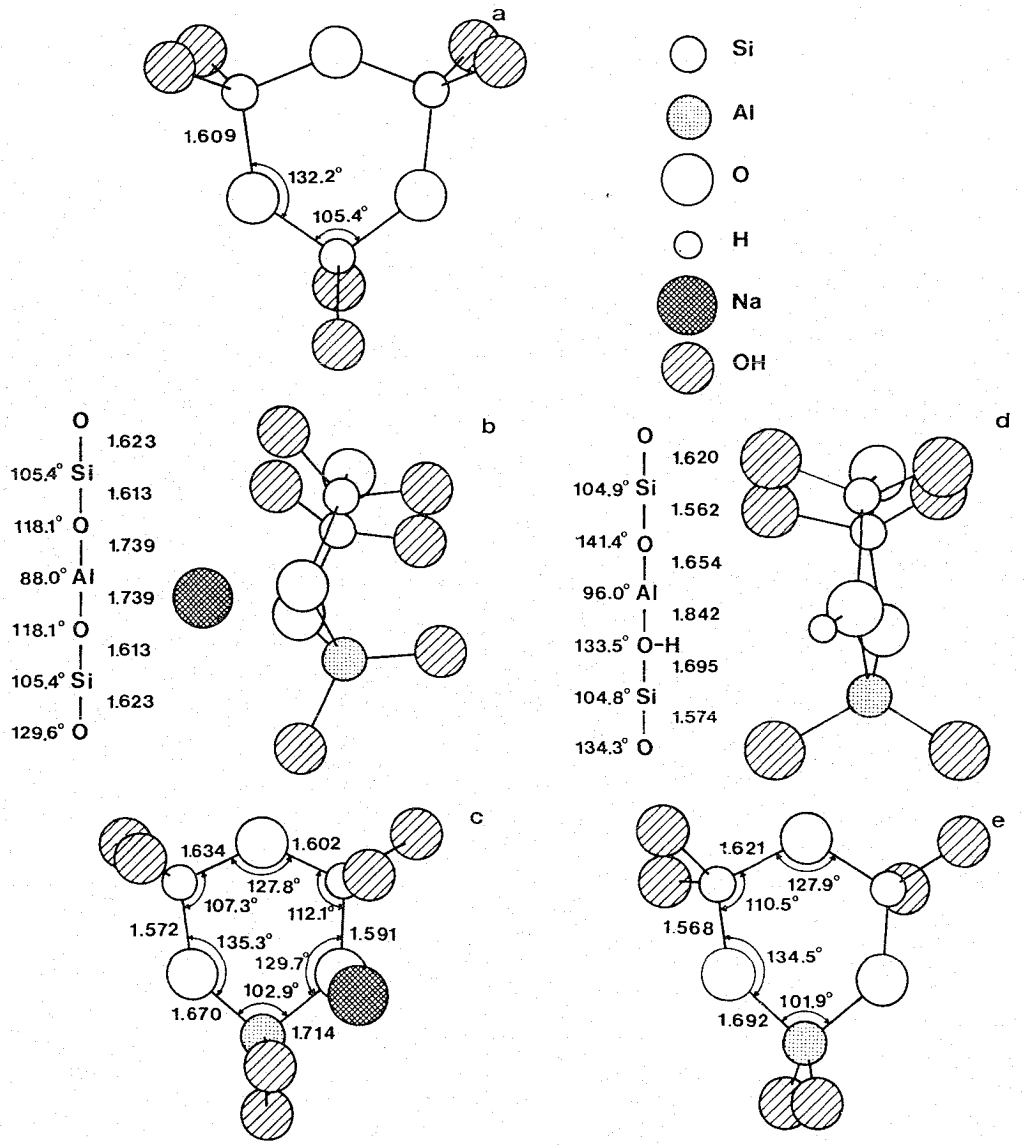

Figure 12. The optimized geometries of the three tetrahedron ring systems (angles in degrees and distances in Å).
a: Aluminumfree ringsystem: $Si_3O_3(OH)_6$ (C_{3v}). Top view.
b: Na-aluminosilicate ring. Na^+ symmetrically coordinated: $AlSi_2O_3(OH)_6^- + Na^+$ (C_s). Side view.
c: Na-aluminosilicate ring. Na^+ asymmetrically coordinated: $AlSi_2O_3(OH)_6^- + Na^+$. Top view.
d: The protonated aluminosilicate ring: $AlSi_2O_3(OH)_6^- + H^+$. Side view.
e: Aluminosilicate ring geometry in the absence of compensating positive charge: $AlSi_2O_3(OH)_6^-$ (C_s). Top view.

sate for the inadequacies of the electrostatic charge distributions in the OH, H or O^- terminated clusters sometimes used.

Noteworthy is the near invariance of the charge on the oxygen atoms if no change occurs in their nearest neighbour coordination. The charge on the Si bridging oxygen atom remains -0.73±0.01 for all clusters. The charge on the Si-Al bridging oxygen atoms becomes -0.83±0.01 in all clusters, except on the oxygen atom to which the proton is coordinated. Now the bridging oxygen charge becomes -0.54, because charge is transferred to the covalently bonded proton. Note that this proton charge is ~0.05 higher than that of the protons of the hydroxyl groups coordinated to Si.

The computed effective charge on the aluminum atoms becomes larger than that on the silicon atoms, because the aluminum atoms have a larger electron donation tendency and a lower formal charge. The charge on the silicon atoms in the aluminosilicate clusters is reduced. This remains also the case for the silicon atom in the tetrahedron that is not bounded with the proton, if the cluster becomes protonated. It illustrates the changes of the charge distribution in a silica tetrahedron due to aluminum substitution in the next tetrahedron. However the changes in the charge distribution are relatively small. As figures 12 show and will be discussed shortly changes in covalent bonding may also contribute to the weaker acidity at high aluminum concentration.

Inspecting figures 12 one observes also that apart from the changes in local electrostatic potential due to altered electron distributions on oxygen atoms sharing the same tetrahedra as the bridging oxygen atoms to which the proton is attached, proton transfer causes significant relaxation of atom distances. The relaxation of distances comparing smaller protonated and non-protonated clusters have also been calculated by Mortier *e.a.*[2i]. As figures 12 show, in comparison to the all silicon cluster, the negatively charged cluster with an aluminum atom has the expected larger Al-O distance (Al-O = 1.692 Å; Si-O = 1.609 Å). The atom distances are slightly altered by the presence of Na^+ ions. The Na^+ ions find minima in two positions. One symmetrically with respect to the cluster (fig. 12b), the other in between an OH group and a bridging oxygen atom (fig. 12c). In the symmetric position the cluster buckles. The bending away of the highly charged cations indicates the importance of electrostatic interactions between the Na ion and Si and Al ions.

The changes in bond lengths are much larger if the cluster becomes bonded to a hydrogen atom (fig. 12d). This is indicative for the strong O-H bond strength, with a resulting weakening of the neighbouring Si-O and Al-O bonds, expected on the basis of Bond Order Conservation[25]. The OH-group is located in the Si-O-Al plane and no buckling of the clusters is seen (fig. 12d) in contrast to the Na^+ case (fig. 12b). Clearly relaxation of the distances and angles upon protonation is important.

Figure 12d shows the long Al-O distance (1.842 Å) if the bridging oxygen atom has the proton attached to it. The other Al-Si tetrahedron bridging oxygen atom has a much shorter Al-O distance (1.65 Å). These changes have been explained above. The Si-O bond sharing the same oxygen atom becomes much shorter than in the aluminumfree ring system (1.56 Å *versus* 1.60 Å). Again because of the Bond Order Conservation principle the other tetrahedron connecting Si-O bond lengthens (1.64 Å *versus* 1.60 Å). If the bridging oxygen atom at the end of this bond would have been connected to another aluminum containing tetrahedron and would be protonated, (the imaginary case not studied here), the weakening of the Si-O bond due to the presence of the other neighbouring aluminum containing tetrahedron would strengthen the OH bond compared to the case that the latter tetrahedron would contain silicon. This implies a lower Brønsted acidity. So surrounding $[_{Si-\overset{H}{O}-Al}]$ sites with aluminum con-

taining tetrahedra will strengthen the OH bond, also because of changes in covalency. The changes in T-O bond length indicate that this may be considerable. Clearly we are dealing with effects of rather short range nature.

Note that the effects of alternating bond lengthening and bond shortening are quantum mechanical. They relate to Friedel oscillations, familiar of impurity scattering in metals[26,27]. The use of classical two body terms would predict a different behaviour from that found in the cluster calculations. The minimal basis set used in our cluster calculations implies that our results have to be considered of qualitative rather than quantitative nature. especially the charges computed will differ if larger basis sets are used.

Whereas bond length and bond angle relaxation may occur also if silica-alumina rings are embedded in a zeolite lattice, restraints may decrease the bond distance relaxation effects found for the free clusters. This has been suggested to be the case in zeolites[1e]. Our calculations however indicate significant driving forces for deformation. The experimentally[28] observed changes in unit cell dimensions of dealuminated zeolite lattices indicate that the zeolite lattice may adjust to the differences in Si-O and Al-O distance. However this may vary for different zeolite lattices (figure 13 and 14).

In systems with little possibility for relaxation, the Si-O-Al angle ϕ may be constrained by its environment, *e.g.* the size of the rings it shares. In such a case hybridization of the oxygen atom electrons depends on the bond angle ϕ[1g,29]. As a result the OH bond strength as well as the oxygen charge are less if the Si-O-Al angle is 180° (sp-hybridization). Hence one expects the higher acidity for the largest bond angles. Indeed, ab-initio calculations by O'Malley and Dwyer[2g] show such a lowering of the bridging OH frequencies in hydrogen terminated Al, Si ditetrahedral clusters with increasing angle ϕ. Beran[1h,1i,1j,1k,1l,1m,1n], using semiempirical methods, found smaller OH dissociation energies in silica-aluminate rings modelling ZSM-5 (five-rings) than faujasite, containing dominantly four-rings. As found from ab-initio calculations[1b]as well as experiment[30,31], the T-O-T angle for the five ring is larger, so indeed on the basis of hybridization arguments a weaker bond is expected. Dwyer[23a] as well as Sohn *e.a.*[28b], using infrared spectroscopy, have shown that dealumination of faujasite structures results in protons with an acidity slightly weaker than that of ZSM-5.

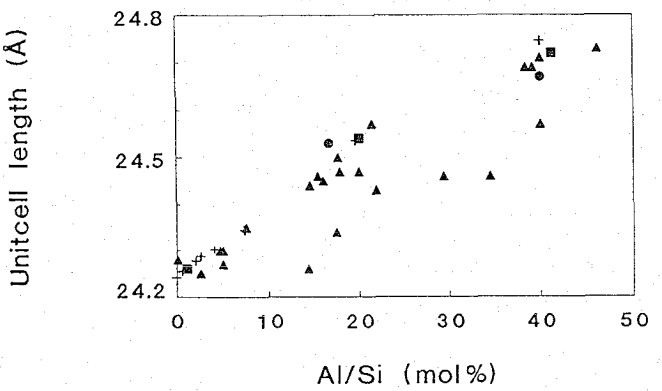

Figure 13. Unit cell dimensions *versus* framework Al/Si ratio for faujasite.
●: ref. 28a; +: ref. 28b; ■: ref. 28c; ▲: ref. 28d.

The arguments presented indicate that in addition to electrostatic contributions to the changes in energy of protonation reactions changes of covalent nature also may

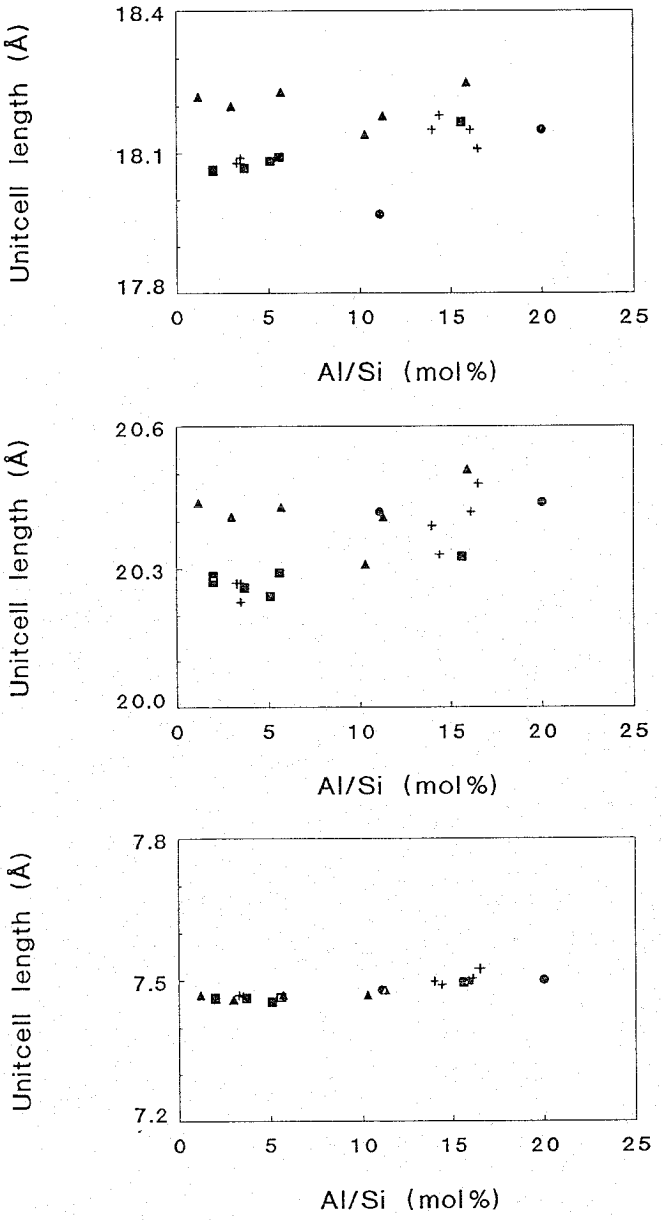

Figure 14. Unit cell dimensions *versus* framework Al/Si ratio for mordenite.
●: ref. 28e; +: ref. 28f; ■: ref. 28g; ▲: ref. 28h.
a: Length of a-axis;
b: Length of b-axis;
c: Length of c-axis;

be significant (see also ref. (20)). Both will be predominantly of a local nature limited to a range of a few lattice atom distances. The presence of cations in the cavity close to the protonation site may also effect protonation. If close they will destabilize the protonated molecule formed in step IV.

According to the view presented zeolite acidity may be affected by four factors:

1: Framework composition;
2: Channel cation composition;
3: Framework relaxability and ring size;
4: Channel dimension.

Our analysis has not considered acidity due to the presence of hydrolizable H_2O [32].

Experimental evidence for the importance of the first two factors is abundant[33]. In the first case changes in lattice oxygen charge occur but also changes in covalent bonding. In the second case destabilization of protonated molecules by the close presence of cations may become important.

Little is known about the presence of lattice strain in zeolites. However proof of lattice relaxation under the influence of adsorbed organic molecules does exist[34]. Stabilization of carbenium ions due to zeolite lattice walls has not yet been demonstrated experimentally. However theoretical (Derouane[35]) as well as experimental evidence (Stach[28c]) is available of lattice wall stabilization of adsorbed organic molecules.

APPENDIX

In this appendix the relation between the formulas of Brüesch[12] for alkali-halides and formulas (5a) and (5b) will be shown.
Also an outline is given of the procedure to be used to extract Z'_{eff} from the calculations.
Brüesch[12] finds for the shell model:

$$\mu\omega_{\text{LO}}^2 = S^* + \frac{8\pi(Z^*e)^2}{3v_a}\frac{1}{1+(8\pi\alpha^*/3v_a)} \tag{A1a}$$

$$\mu\omega_{\text{TO}}^2 = S^* - \frac{4\pi(Z^*e)^2}{3v_a}\frac{1}{1-(4\pi\alpha^*/3v_a)} \tag{A1b}$$

With the relation of Clausius-Mosotti (9), these two relations can be rewritten as:

$$\mu\omega_{\text{LO}}^2 = S^* + \frac{8\pi(Z^*e)^2}{3v_a}\frac{(\epsilon(\infty)+2)}{3\epsilon(\infty)} \tag{A2a}$$

$$\mu\omega_{\text{TO}}^2 = S^* - \frac{4\pi(Z^*e)^2}{3v_a}\frac{(\epsilon(\infty)+2)}{3} \tag{A2b}$$

We wish to rewrite formulas (A2a) and (A2b) in the form

$$\mu\omega_{\text{LO}}^2 = S' + \frac{8\pi(Z'_{\text{eff}}e)^2}{3v_a\epsilon(\infty)} \tag{A3a}$$

$$\mu\omega_{\text{TO}}^2 = S' - \frac{4\pi(Z'_{\text{eff}}e)^2}{3v_a\epsilon(\infty)} \tag{A3b}$$

These formulas are equal to (5a) and (5b).

Substracting (A2b) from (A2a) and (A3b) from (A3a) gives:

$$\mu\omega_{\mathrm{LO}}^2 - \mu\omega_{\mathrm{TO}}^2 = \frac{4\pi(Z^*e)^2}{9v_a}\frac{(\epsilon(\infty)+2)^2}{\epsilon(\infty)} = \frac{4\pi(Z'_{\mathrm{eff}}e)^2}{v_a\epsilon(\infty)} \tag{A4}$$

so one obtains an expression for Z'_{eff}:

$$(Z'_{\mathrm{eff}})^2 = \left(\frac{(\epsilon(\infty)+2)Z^*}{3}\right)^2 \tag{A5}$$

Z'_{eff} is also called the *transverse effective charge*, Z^* is known as the *Szigeti charge*. Adding formula (A2a) and two times (A2b), and (A3a) and two times (A3b) respectively, results in:

$$\mu(\omega_{\mathrm{LO}}^2 + 2\omega_{\mathrm{TO}}^2) = 3S^* + \frac{8\pi(Z^*e)^2}{3v_a}\frac{(\epsilon(\infty)+2)}{3}\frac{(1-\epsilon(\infty)}{\epsilon(\infty)} = 3S' \tag{A6}$$

finally giving

$$S' = S^* + \frac{8\pi(Z^*e)^2}{9v_a}\frac{(\epsilon(\infty)+2)}{3}\frac{(1-\epsilon(\infty)}{\epsilon(\infty)} \tag{A6}$$

So one derives that it is possible to put the shell model formulas (A1a) and (A1b) of Brüesch in a form (formulas (5a) and (5b)) that is very similar to the rigid ion model formulas (4a) and (4b).

The equations given above apply to diatomic cubic systems. In a more general case the plasmon frequency $\omega_{\mathrm{plasmon}}$ is given by[36]:

$$\langle\omega_{\mathrm{LO}}^2\rangle - \langle\omega_{\mathrm{TO}}^2\rangle = \frac{4\pi}{v_a\epsilon(\infty)}\sum_i \frac{(Z'_{\mathrm{eff}})_i^2 e^2}{m_i} = \omega_{\mathrm{plasmon}}^2 \tag{A7}$$

where $(Z'_{\mathrm{eff}})_i$ and m_i are the effective charge and the mass of ion i, respectively, and the summation runs over all the ions in the unit cell. Equation A7 can be rewritten as

$$\langle\omega_{\mathrm{LO}}^2\rangle - \langle\omega_{\mathrm{TO}}^2\rangle = \frac{4\pi(Z'_{\mathrm{eff}})^2}{\mu' v_a\epsilon(\infty)} = \omega_{\mathrm{plasmon}}^2 \tag{A8}$$

where μ', **not** the ordinary reduced mass, is fixed for a given stoichiometry. The ratio Z'_{eff}/Z can now be obtained from a combination of a rigid ion and a shell model phonon calculation.

$$\frac{(\langle\omega_{\mathrm{LO}}^2\rangle - \langle\omega_{\mathrm{TO}}^2\rangle)^{\mathrm{shell}}}{(\langle\omega_{\mathrm{LO}}^2\rangle - \langle\omega_{\mathrm{TO}}^2\rangle)^{\mathrm{rigid}}} = \frac{1}{\epsilon_L(\infty)^{\mathrm{shell}}}\frac{(Z'_{\mathrm{eff}})^2 v_a^{\mathrm{rigid}}}{Z^2 v_a^{\mathrm{shell}}} \tag{A9}$$

Because the relaxed lattice is different for the rigid ion and shell model calculations two different values of v_a are used. The results of these calculations are given in table 1.

References

1a M.D. Newton, M. O'Keeffe, and G.V. Gibbs, Phys. and Chem. of Miner. 6:305 (1980).

b B.W.H. van Beest, J. Verbeek, and R.A. van Santen, Catal. Lett. 1:147 (1988).
c J.G. Fripiat, F. Berger-André, J. André, and E.G. Derouane, Zeolites 3:306 (1983).
d J. Sauer, and R. Zahradnik, Int. J. Quantum Chem. 26:793 (1984).
e A.G. Pelmenshchikov, E.A. Paukshtis, V.S. Stepanov, K.G. Ione, G.M. Zhidomirov, and K.I. Zamaraev, in: "Proc. 9th Int. Congr. on Catalysis," M.J. Philips and M. Ternane ed., The Chemical Institute of Canada, 1:404 (1988).
f G.M. Zhidomirov, and V.B. Kazansky, Adv. Catal. 34:131 (1986).
g G. Ooms, and R.A. van Santen,. Recl. Trav. Chim. Pays Bas 106:69 (1987).
h S. Beran, P. Jírů, and B. Wichterlová, J. Phys. Chem. 85:1951 (1981).
i S. Beran, J. Phys. Chem. 85:1956 (1981).
j S. Beran, P. Jírů, B. Wichterlová, React. Kinet. Catal. Lett. 18:51 (1981).
k S. Beran, J. Phys. Chem. 86:111 (1982).
l S. Beran, Chem. Phys. Lett. 91:86 (1982).
m S. Beran, Z. Phys. Chem. Neue Folge 130:81 (1982).
n S. Beran, Z. Phys. Chem. Neue Folge 137:89 (1983).
p G.V. Gibbs, Amer. Miner. 67:421 (1982).
2a J. Sauer, J. Phys. Chem. 91:2315 (1987).
b J. Sauer, and W. Shirmer, Stud. Surf. Sci. Catal. 37:323 (1988).
c E. Kassab, K. Seiti, and M. Allavena, J. Phys. Chem. 59 (1989), in press.
d V.B. Kazansky, Bulg. Acad. of Sciences Comm. Rep. Chem. 13:19 (1980).
e P.J. O'Malley, and J. Dwyer, Chem. Phys. Lett. 143:97 (1988).
f P.J. O'Malley, and J. Dwyer, Zeolites 8:317 (1988).
g P.J. O'Malley, and J. Dwyer, J. Phys. Chem. 92:3005 (1988).
h W.J. Mortier, P. Geerlings, C. van Alsenoy, and H.P. Figeys, J. Phys. Chem. 83:3257 (1979).
i W.J. Mortier, J. Sauer, J.A. Lercher, and H. Noller, J. Phys. Chem. 88:905 (1984).
j R. Vetrivel, C.R.A. Catlow, and E.A. Colbourn, Stud. Surf. Sci. Catal. 37:309 (1988).
k R. Vetrivel, C.R.A. Catlow, and E.A. Colbourn, to be published.
l I.D. Mikheikin, I.A. Abronin, G.M. Zhidomirov, and V.B. Kazansky, Kinet. Katal. 18:1580 (1977).
m I.D. Mikheikin, I.A. Abronin, A.I. Lumpuv, and G.M. Zhidomirov, Kinet. Katal. 19:1050 (1978).
n K. Seiti, Thesis, Univ. Paris VI, 1988.
p K.A. van Genechten, Thesis Univ. Leuven (1987).
q K.A. van Genechten, and W.J. Mortier, Zeolites 8:273 (1988).
3a G. Ooms, R.A. van Santen, C.J.J. den Ouden, R.A. Jackson, and C.R.A. Catlow, J. Phys. Chem. 92:4462 (1988).
b E. Dempsey, J. Phys. Chem. 75:3660 (1969).
c C.R.A. Catlow, and W.C. Mackrodt, "Computer Simulation of Solids," Lecture Notes on Physics, Springer Verlag, Berlin (1982).
d G. Ooms, R.A. van Santen, R.A. Jackson, and C.R.A. Catlow, Stud. Surf. Sci. Catal. 37:317 (1988).
e M.J. Sanders, "Computer Simulation of Framework Structured Minerals," PhD Thesis Univ. of London (1984).

f R.A. Jackson, and C.R.A. Catlow, Molec. Simulation 1:207 (1988).
g A.J.M. de Man, B.W.H. van Beest, M. Leslie, and R.A. van Santen, submitted.
h C.R.A. Catlow, M. Doherty, G.D. Price, M.J. Sanders, and S.C. Parker, Mater. Sci. Forum, 7:163 (1986).
4 C. Pisani, R. Dovesi, and C. Roetti, "Hartree-Fock ab initio treatment of crystalline systems," Lecture Notes in Chemistry 48, Springer Verlag, Berlin (1988).
5 A. Goursot, F. Fajula, C. Daul, and J. Weber, J. Phys. Chem 92:4456 (1988).
6a C.S. Blackwell, J. Phys. Chem. 83:3251 (1979).
b C.S. Blackwell, J. Phys. Chem. 83:3257 (1979).
c P. Demontis, G.B. Suffritti, S. Quartieri, E.S. Fois, and A. Gamba, Zeolites 7:522 (1987).
d P. Demontis, G.B. Suffritti, S. Quartieri, E.S. Fois, and A. Gamba, J. Phys. Chem. 92:867 (1988).
e K.T. No, D.H. Bae, and M.S. Jhon, J. Phys. Chem. 90:1772 (1986).
7 M. Mabilia, R.A. Pearlstein, and A.J. Hopfinger, J. Am. Chem. Soc. 109:7960 (1987).
8 R.A. van Santen, and D.L. Vogel, Adv. Solid State Chem. I:151 (1988).
9 R. Haydock, V. Heine, and M.J. Kelley, J. Phys. C: Solid State Physics 5:2845 (1972).
10 R. Haydock, V. Heine, and M.J. Kelley J. Phys. C: Solid State Physics 8:2591 (1975).
11 J. Etchepare, and M. Marian, J. Chem. Phys. 60:1873 (1974).
12 P. Brüesh, "Phonons: Theory and experiments. I," Springer Series Solid State Sciences 34, Springer Verlag, Berlin (1982).
13 A.A. Maraduddin, E.W. Montroll, G.H. Weiss, and I.P. Ipatova "Theory of lattice dynamics in the harmonic approximation", Academic Press, New York (1971).
14 S. Tsuneyuki, M. Tsukada, H. Aoki, and Y. Matsui, Phys. Rev. Letters 61:869 (1988).
15 G.J. Kramer, and A.J.M. de Man, unpublished results.
16 M.E. Striefler, and G.R. Barsch, Phys. Rev. B 12:4553 (1975).
17 G.K. Johnson, I.R. Tasker, D.A. Howell, and J.V. Smith, J. Chem. Thermodynamics 19:617 (1987).
18 J. Patarin, M. Soulard, H. Kessler, J.L. Guth, and M. Diot, Thermochimica Acta, in press.
19 R.A. van Santen, Recl. Trav. Chim. Pays-Bas 101:157 (1982).
20 C.E. Dijkstra, Acc. Chem. Res. 21:355 (1988).
21 J. Woning, and R.A. van Santen, Chem. Phys. Lett. 101:541 (1983).
22 H.M. Evjen, Phys. Rev. 39:675 (1932).
23a J. Dwyer, Stud. Surf. Sci. Catal. 37:333 (1988).
b P.A. Jacobs, Catal. Rev.-Sci. Eng. 24:415 (1982).
24 B.W.H. van Beest, J. van Lenthe, and R.A. van Santen, to be published.
25 E. Shusterovich, Surf. Sci. Rep. 6:1 (1986).
26 R.A. van Santen, J. Chem. Soc. Faraday Trans. 83:1915 (1987).
27 J. Friedel, Nuovo Cimento Suppl. 7:286 (1958).
28a P. Gallezot, R. Beaumont, and D. Barthomeuf, J. Phys. Chem. 78:1550 (1974).
b J.R. Sohn, S.J. DeCanio, J.H. Lunsford, and D.J. O'Donnel, Zeolites 6:225 (1986).
c H. Stach, U. Lohse, H. Thamm, and W. Schirmer, Zeolites 6:74 (1986).

d L. Kubelková, V. Seidl, G. Borbély, and H.K. Beyer, J. Chem. Soc. Faraday Trans. 84:1447 (1988).
e B.H. Ha, J. Guidot, and D. Barthomeuf, J. Chem. Soc. Faraday Trans. I 75:1245 (1979).
f R.W. Olsson, and L.D. Rollmann, Inorganic Chemistry 16:651 (1977).
g B.L. Meyers, T.H. Fleisch, G.J. Ray, J.T. Miller, and J.B. Hall, J. Catalysis 110:82 (1988).
h M. Musa, V. Tarină, A.D. Stoica, E. Ivanov, E. Ploştinaru, E. Pop, Gr. Pop, R. Ganea, B. Bîrjega, G. Muscă, and E.A. Paukshtis, Zeolites 7:427 (1987).
29 J.R. Durig, M.J. Flanigan, and V.F. Kalasinsky, J. Chem. Phys. 66:2775 (1977).
30 C. Baerlocher, in: "Proc. 6^{th} Int. Zeol. Conf. Reno," 823 (1983).
31 W.H. Baur, Amer. Miner. 49:697 (1964).
32 P.A. Jacobs, "Carboniogenic Acidity of Zeolites," Elsevier, (1977).
33 P.A. Jacobs, and W.J. Mortier, Zeolites 2:226 (1982).
34a J. Klinowski, Progr. NMR Spectr. 16:237 (1984).
b C.A. Fyfe, H. Strobl, G.T. Kokotailo, G.J. Kennedy, and G.E. Barlow, J. Am. Chem. Soc. 110:3373 (1988).
35a E.G. Derouane, J. Catal. 100:541 (1986).
35b E.G. Derouane, J.M. André, and A.A. Lucas, J. Catal. 110:58 (1988).
36 M.F. Thorpe, and S.W. de Leeuw, Phys. Rev. B 33:8490 (1986).